Y. Katano

M. Ando

T. Itoh

M. Sasaki

Nissan Research Center,
Nissan Motor Co., Ltd.,
1, Natsuhima-cho, Yokosuka, 237 Japan

Application of Ceramics to Turbocharger Rotors for Passenger Cars

Nissan has been developing and marketing ceramic turbocharger rotors for five years. This paper outlines the major theories and techniques used in ceramic fabrication, joining of ceramic and metal components, and machining of ceramics. It also presents a dynamic stress analysis using DYNA3D and describes techniques used in performing impact damage experiments, reliability evaluation, and lifetime prediction.

Introduction

The adoption of stringent emission standards in Japan in the latter half of the 1970s led to a reduction in power output for many Japanese passenger car engines. To recover lost engine power, there was a strong need to maximize the efficiencies of small engines while minimizing price increases. Another factor that had to be considered was the hefty tax assessed at that time on engines having a displacement over 2.0 liters.

One answer to that situation was the use of a turbocharging system, which is a rather common means of increasing engine output and can be applied without making many modifications to main engine components and systems. Metal turbochargers were first applied to various classes of Nissan cars beginning around 1978. However, there was a growing demand to improve the acceleration response of the turbocharger, which is one of the main demerit is of turbocharging. One effective method for overcoming this problem of turbo lag is to reduce the moment of inertia of the turbocharger rotor, which can be accomplished through the use of ceramics.

Nissan has conducted research on experimental turbine rotors for use in ceramic gas turbines since the company started spin tests of ceramic disks toward the end of the 1970s. A high-efficiency ceramic turbocharged engine was released in 1985 and has been used in more than 400,000 passenger cars to date (Fig. 1). In connection with the redesign and modification of the turbocharger, three types of ceramic rotors have been developed so far (Fig. 2).

The CN-1 type [1] was produced between 1985 and 1987 and was used with 2.0-liter in-line six-cylinder DOHC engines. The CNR-1 type [2, 3] has been in production since 1987. This ceramic rotor is a redesigned, low-stress version of the CN-1 and is used with 2.0 liter in-line six-cylinder or V-6 DOHC engines and 3.0-liter V-6 DOHC engines [4]. It features water passages provided in the bearing housing and ball bearings instead of plain journal bearings. A thrust bearing was also subsequently adopted [5]. The T-25 type has been in production since 1989 and was developed for use with 2.6-liter twin-turbocharged in-line six-cylinder DOHC engines [6]. The design details of this ceramic rotor are explained in [1, 2], and the engine performance obtained is described in [1, 3, 4, 6].

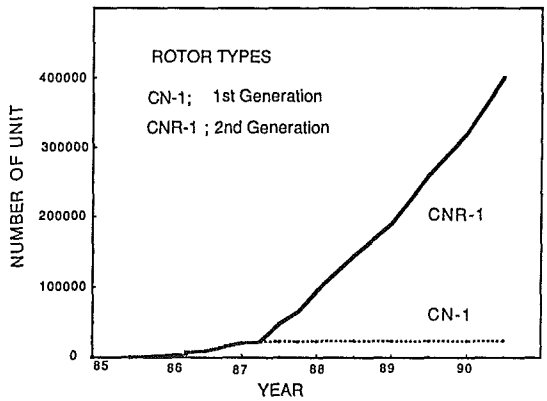

Fig. 1 Number of vehicles equipped with ceramic turbocharger rotors

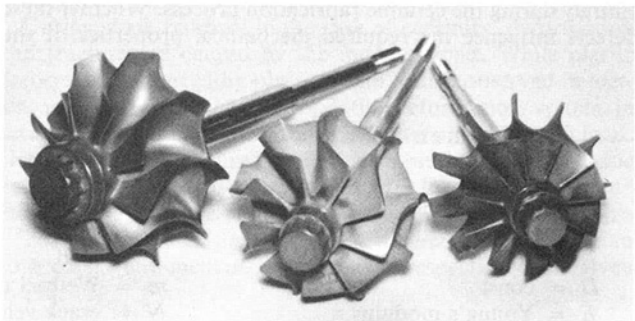

Fig. 2 Three types of ceramic turbocharger rotors: left: CN-1, center: CNR-1, right: T-25

Contributed by the International Gas Turbine Institute and presented at the 36th International Gas Turbine and Aeroengine Congress and Exposition, Orlando, Florida, June 3–6, 1991. Manuscript received at ASME Headquarters March 4, 1991. Paper No. 91-GT-264. Associate Technical Editor: L. A. Riekert.

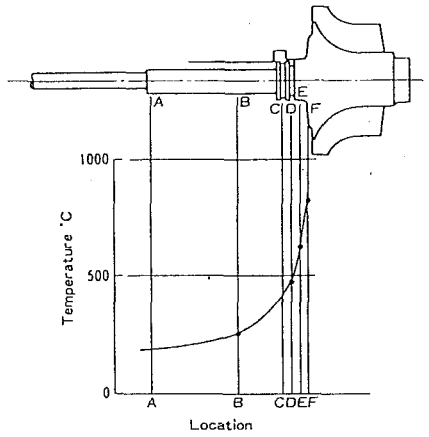

Fig. 3 Temperature distribution in turbine rotor shaft during heat soak-back

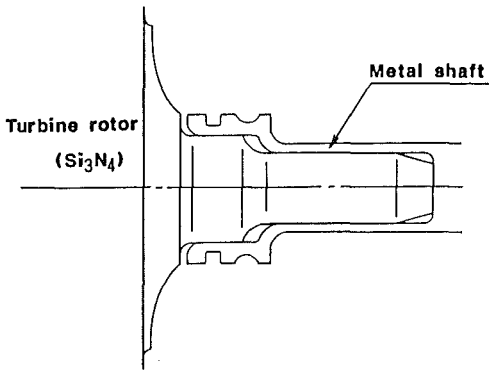

Fig. 4 Design of bonding method (double shrink-fitting

A turbocharger rotor must be capable of withstanding long periods of use in automobile exhaust gas, which can reach temperatures as high as approximately 900°C. Ceramic materials, which are inherently brittle, have been applied to automobile structural parts that require high reliability and durability. This paper describes some of the techniques for applying ceramics to structural components, using the turbocharger rotor as an example.

Ceramic Materials and Fabrication Process

Ceramic Materials. Silicon nitride was chosen as the rotor material because of its strength, fracture thoughness, thermal shock resistance, and thermal expansion coefficient [1, 2]. Generally, covalent silicon nitride is not interable, but is rendered so through the use of common sintering aids such as Y_2O_3 and Al_2O_3.

Raw Materials—Silicon Nitride and Sintering Aids. It is impossible to avoid the occurrence of pores and other defects entirely during the ceramic fabrication process. Whether these defects influence the required mechanical properties of the ceramic depends on the stress conditions. Nonetheless, defects must be eliminated as much as possible.

Molding Methods. Molding methods are limited to injection molding and slip casting for a complex geometry like that of a turbine blade. Voids are generally spherical in slip-cast ceramic bodies, but have a sharp form in injection molded bodies. Slip casting has the advantage that stress concentrations, which are caused by spherical voids, are less likely to occur. However, at Nissan we had selected injection molding because it is better suited to mass production.

The injection molding process consists of several operations, including the mixing of the ceramic powder and organic binder, injection molding and binder removal. Mutsuddy and Shetty have presented a detailed report of the injection molding process [7].

Sintering Methods. Densification methods for silicon nitride include reaction sintering, normal sintering, hot pressing, and gas pressure sintering.

In reaction sintering, the silicon powder compacted body is densified by nitridation (reaction of Si with N_2 to Si_3N_4). The sintered body does not have sufficient strength, but dimensional accuracy is maintained during sintering. With hot pressing, the compact body is densified with the help of mechanical pressure applied along one axis. This method, however, is unsuitable for a complex geometry like that of turbine blades. Normal sintering is performed under 1 atm pressure in a nitrogen gas atmosphere. It is thought that thermal decomposition occurs around the sintering temperature, which is usually above 1800°C. Gas pressure sintering is performed under high pressure in a nitrogen gas atmosphere. This method is most suitable for fabrication of a high-density sintered ceramic body.

Gas pressure sintering and normal sintering under well-controlled conditions are thought to be the best sintering methods for ceramic turbocharger rotors.

Joining Technology

The technology for joining the ceramic rotor and steel shaft was a key element in the development of ceramic turbochargers. The two components are joined just under the ring seal pit, where the temperature rises to 450°C for an uncooled housing during heat soak-back, which causes the highest temperatures. An example of the temperature distribution during heat soak-back is shown in Fig. 3. The position for the soak-back is shown in Fig. 3. The position for the ceramic-steel joint was selected for the following reasons: (1) to reduce the possibility of lubricating oil leakage from the bearing to the exhaust pipe; (2) to increase rotor reliability by reducing the effective rotor volume; (3) to reduce production cost. The location chosen, however, presents the severest conditions for joining. For the turbochargers developed to date, mechanical joining has been accomplished using a shrink-fitting method and chemical joining has been effected through an active brazing technique.

A cross section of the steel shaft and ceramic rotor joint formed by shrink-fitting is illustrated in Fig. 4. In an earlier design, a double shrink-fitting method was employed to assure

Nomenclature

A = premultiplier in crack velocity
a = crack length
B = const
D = const
E = Young's modulus
F = failure probability
H = hardness
Kc = fracture toughness
K_{IC} = critical stress intensity factor
L = load
m = Weibull modulus
N = crack velocity exponent
P = survival probability
r = radius
S = material strength
t = time
V = velocity
v_e = effective volume
Y = shape factor
ρ = density
σ = stress

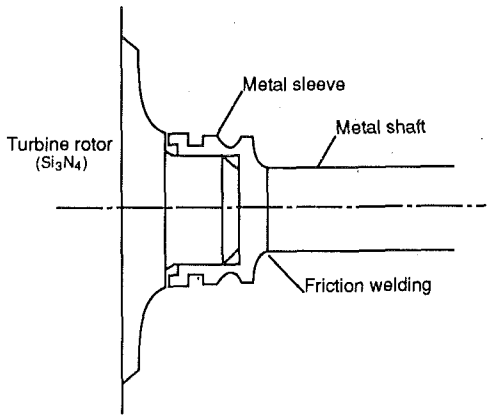

Fig. 5 Design of bonding method (shrink-fitting)

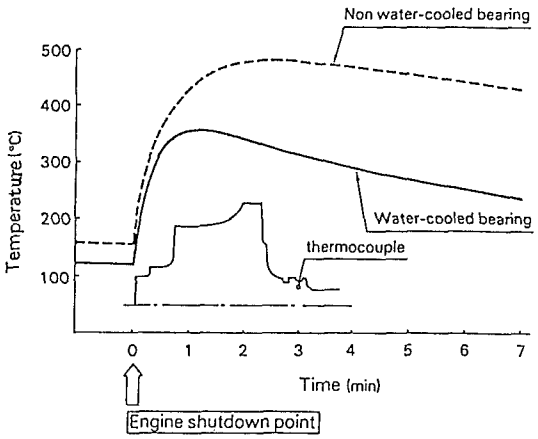

Fig. 6 Temperature of ceramic-to-metal joint during heat soak-back

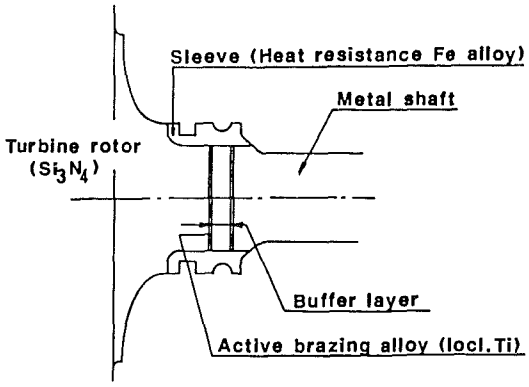

Fig. 7 Design of bonding method (active brazing)

reliability by enhancing the bonding strength. With a more recent design, a simpler shrink-fitting technique has been adopted to facilitate the use of a water-cooled bearing [8], which is shown in Fig. 5. The temperature distributions during heat soak-back for a turbocharger rotor equipped with a water-cooled bearing and one without are given in Fig. 6 [3]. While this shrink-fitting method is simple, it requires micron-order machining accuracy to maintain the bonding strength between the steel shaft and ceramic rotor.

A cross-sectional view of a joint formed by active brazing is shown in Fig. 7. This method employs an active brazing alloy containing titanium. A buffer layer, composed of Ni and W, is also provided between the ceramic rotor and steel shaft. Brazing is performed in only one heating process. A finite element analysis of a joint formed by active brazing indicates

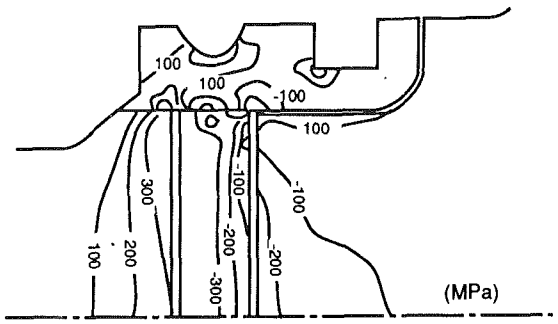

Fig. 8 Residual stress distribution in ceramic rotor

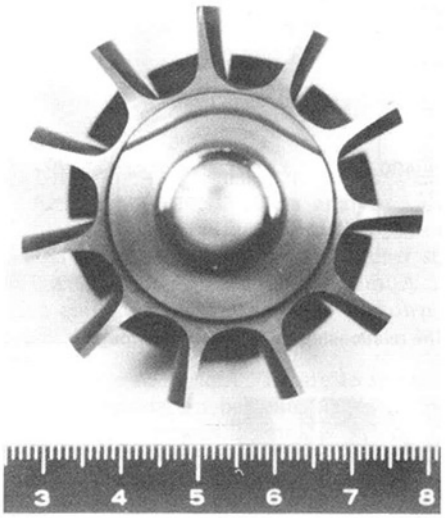

Fig. 9 Ceramic back hub plate after machining for balance

that the provision of a buffer layer reduces the residual stresses as compared with the direct brazing of silicon nitride and steel. Figure 8 shows the stress analysis results obtained with an elastic/plastic model for a joint formed by a silicon nitride rotor with a buffer layer and a steel shaft overlaid with a heat resistant steel having a low thermal expansion coefficient [9].

Machining Techniques for Ceramics

There are two reasons why it is important to study the machining techniques for ceramics. The first is that the machining process for the turbocharger rotor accounts for the greatest position of the total rotor production cost. This is also true for other ceramic components. The second reason is that the residual damage induced during machining degrades the mechanical strength of ceramics. One of the most commonly used machining processes for ceramics to date has been grinding, which is utilized to correct the rotational balance of the turbocharger rotor (Fig. 9) and will be discussed in this section.

During stock removal in the case of ceramics, deformation and fracture are caused by the indenter load. While plastic deformation induced by plastic strain is also observed in metals, regardless of other factors, the deformation system in ceramics differs depending on the indenter radius and load. Hertzian cracks [10] are initiated by a blunt indenter, plastic deformation is caused by a low indenter load, and a median/radial crack system is induced by a high indenter load [11].

The critical loads (Le and Lp) for the initiation of Hertzian cone cracks and median/radial cracks, respectively, are given as [10, 12]

$$Le = De \cdot r \cdot Kc^2/E \quad (1)$$

$$Lp = Dp \cdot Kc^4/H^3 \quad (2)$$

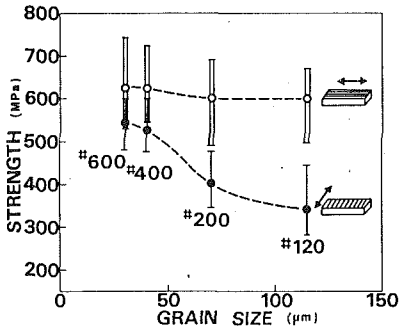

Fig. 10 The relationship between grain size and strength

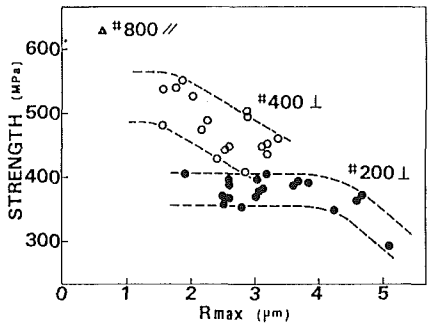

Fig. 11 The relationship between surface roughness and strength

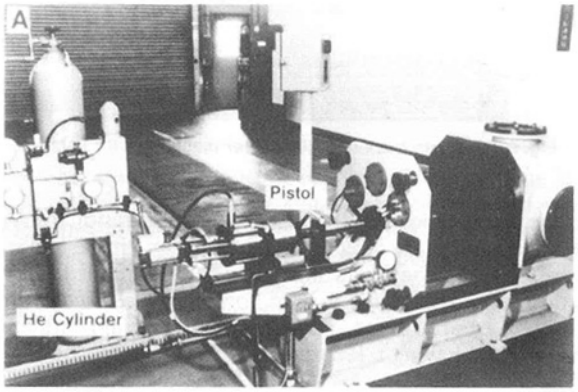

Fig. 12 Experimental apparatus

where De and Dp are dimensionless constants, r is the indenter radius, Kc is the material fracture toughness, E is the Young's modulus, and H is the hardness. In the case of machining, where the indenter is assumed to be a grain of a diamond grinding wheel and Lp is much smaller than Le [10], the median/radial crack size becomes the important factor. The relationship between the indenter load and material fracture toughness is given as [11]

$$L/a^{3/2} = B \cdot Kc \tag{3}$$

where a is the crack length and B is a dimensionless constant, which becomes smaller with a narrower indenter tip radius [13]. Equation (3) indicates that lower fracture toughness and lower indenter loads result in larger cracks.

It is generally acknowledged that the machinability of a material is related to its fracture toughness, hardness, and strength. Evans et al. [14] reported that the stock removal speed, V, varies according to the material parameters Hv and Kc, and proposed the following equation:

$$V \propto L^{5/4} \cdot H^{-1/2} \cdot Kc^{-3/4} \tag{4}$$

where L is the load applied perpendicular to the wheel radius. Stored elastic strain energy, used as an index of machinability, becomes larger for materials with low E and large σ, resulting in lower machinability. This suggests that commercially available silicon nitride has low machinability [15].

As noted earlier, surface cracks induced in ceramics during machining are a major cause of strength degradation. It is essential to understand the effect of machining damage on strength degradation of ceramics in structural applications requiring high reliability. Experiments were conducted to examine the relationship between machining and material strength. Silicon nitride specimens were ground along their longitudinal and lateral axes using diamond grinding wheels of different grain size. After grinding, the surface roughness and strength of 20 specimens were measured. In Fig. 10, residual strength is shown as a function of grain size for both grinding directions. The results clearly show that strength degradation increased with a larger grain size for grinding in the lateral direction. The fracture origin is thought to be the grinding track and/or cracks generated just below the grinding track. As strength degradation increased with a larger grain size, the track length became larger [16].

The results in Fig. 11 show residual strength as a function of surface roughness. There is some correlation between surface roughness and residual strength resulting from the grain size of the grinding wheel used. In reality, residual strength is determined by the crack size just below the grinding track and so the relationship between surface roughness and strength is thought to be provisional. While residual strength is an important factor in stress simulation, the effect of residual strength on reliability is also considerable.

Impact Damage to Silicon Nitride

Ceramics are inherently brittle and cracks caused by point indentations have been reported to lead to catastrophic failure [17]. In-service examples of this behavior include the failure of aircraft turbine blades caused by ingestion of solid particles [18] and Hertzian cone cracks in helicopter windshields resulting from flotation of solid particles [19]. Results of a model analysis also indicate impact damage to the glassy coating of the heat shield tiles used on the space shuttles [20]. These phenomena have been studied and analyzed using Hertzian cone-fracture theory [21]. In the case of turbine blades in automotive turbochargers, it is thought that oxide scale, particles of welding beads, and residual particles of casting sand can become the cause of catastrophic failure.

Extensive studies have been made of the impact damage to silicon nitride for the purpose of assuring durability of automotive turbocharger rotors made of this ceramic [22]. In the course of developing ceramic rotors at Nissan, impact damage behavior was examined in basic model tests and durability testing was done. The results were then used in designing the turbocharger rotors. Analyses were made of the blade thickness and damage effects of different impactors were also examined in developing practical silicon nitride ceramics for rotor application [22]. Computer simulations were also performed to analyze the stress level [23] and finally the fabricated rotors were subjected to durability tests.

Model Impact Test. Commercially available gas-pressure-sintered silicon nitride was obtained from NGK Spark Plug CO., Ltd. Partially stabilized zirconia (PSZ) spheres 1.0 mm in diameter were obtained from Toso Co., Ltd. and used in impact tests to represent oxide scale, casting sand, and steel particles of welding beads. The silicon nitride specimens, measuring 50 × 8 × 3 mm, 50 × 8 × 2 mm, and 50 × 8 × 1 mm, were polished with two grades of diamond paste (6 μm and 3 μm) to eliminate surface machining damage. The specimens were oriented perpendicularly to the approach direction. A helium gas gun (Fig. 12) was used to fire the particles at velocities ranging from 100 -330 m/s. After the impact tests,

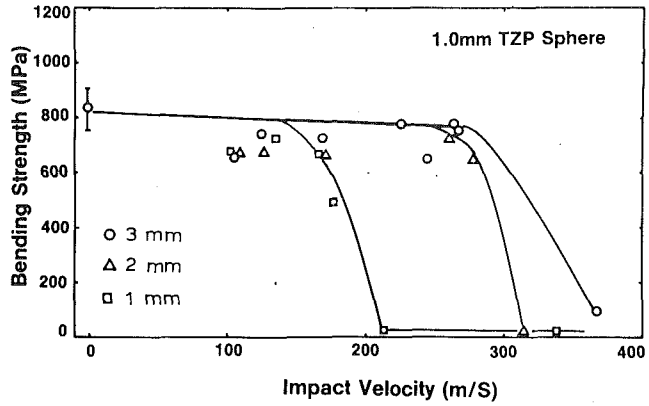

Fig. 13 Post-impact bending strength showing different strength degradation trends for different blade thicknesses

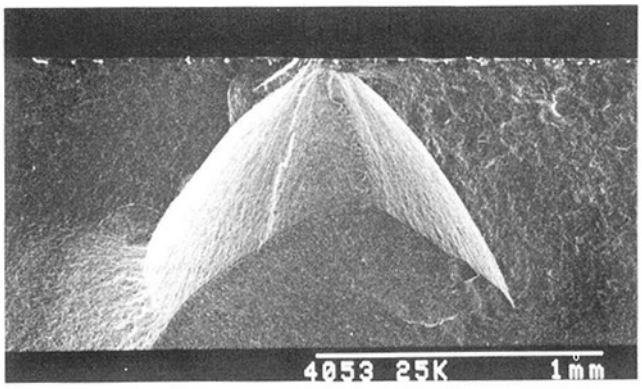

Fig. 14 Hertzian cone crack initiated at the fractured surface

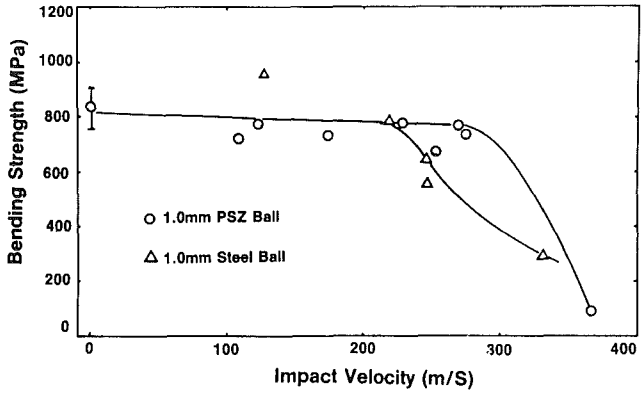

Fig. 15 Post-impact bending strength showing different strength degradation trends for different impactors (specimen thickness = 3 mm)

the residual strength was measured in a four-point bending test (inner span: 10 mm, outer span: 30 mm) at a crosshead speed of 0.5 mm/min. Fractured surfaces were examined by scanning electron microscopy (SEM).

Effect of Turbine Blade Thickness. The postimpact bending strength of the silicon nitrides specimens is shown in Fig. 13 as a function of the impact velocity for three blade thicknesses. For the 2- and 3-mm-thick blades, strength was maintained nearly up to an impact velocity of 290 m/s, when a sudden drop occurred. The PSZ spheres were crushed at a speed of 200 m/s. The bending strength of the 1-mm-thick blade decreased rapidly below 200 m/s. A Hertzian cone crack [21] connected to a surface ring crack was generated in the specimen resulting in strength degradation. This result suggested that impact damage initiated Hertzian cone cracks more

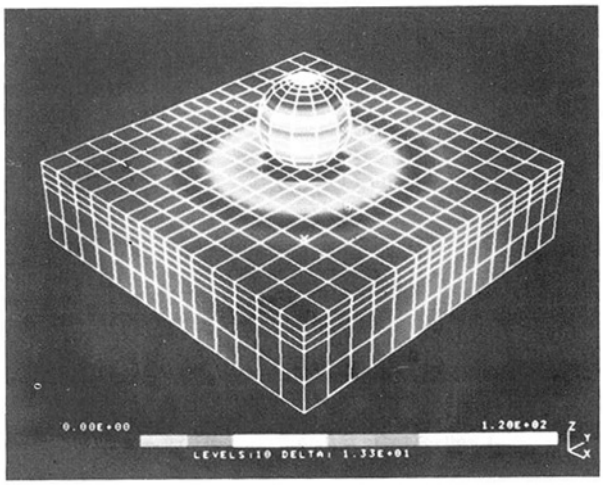

Fig. 16 FEM stress analysis using DYNA3D

easily in the 1-mm-thick specimen than in the 2- or 3-mm-thick specimens. Although a precise stress analysis was not conducted, it is thought that the effect of crack initiation, in terms of the reflected stress wave, caused much higher stress in the 1-mm-thick specimen than in the thicker ones. A micrograph of a Hertzian cone crack in the GPSSN is shown in Fig. 14 for a 3-mm-thick specimen.

Effect of Impactor Materials. Figure 15 shows the difference in strength degradation behavior for two different impactors. With the PSZ spheres, strength degradation occurred at 290 m/s, similar to the results seen in Fig. 13. With the metal impactors, a Hertzian cone crack was initiated in the specimens, although only slight damage was observed on the surface. The crack initiation velocity was lower than in the case of the PSZ spheres. In this case, plastic deformation on the target was not observed. It is presumed that the sphere was probably deformed when the impact load was fully translated to the target, resulting in the generation of a Hertzian stress field. The critical impact velocity of the two types of sphere was accurately compared using the following equation proposed by Wiederhorn and Lawn [24]:

$$Vc_1/Vc_2 = (\rho_2/\rho_1)^{1/2} \quad (5)$$

The subscripts land 2 denote ceramics and metal, respectively. The calculation and experimental results agreed well in a ratio of 1.14.

Dynamic Stress Analysis using DYNA3D. The Hertzian cone crack theory [21] is usually applied to an analysis of fracture behavior resulting from a spherical particle impact. In this work, a dynamic stress analysis was performed using DYNA3D developed by Halloquist [23]. The FEM model was structured with a target size of 4 × 4 × 1 mm, using 1125 hexagonal solid elements to express the target, and a sphere diameter of 1 mm, using 816 pentagonal and hexagonal elements to represent the sphere.

The location of maximum principal stress at 0.6 μs after impact is shown in Fig. 16. The maximum stress level (ring shape) is equivalent to the material strength level at a 90-deg impact angle. Its direction is the same as σ_{22} and it is caused by σ_{11}. It corresponds to a ring crack at the top of a Hertzian cone crack. The Hertzian cone crack is though to extend inward along the σ_{33} direction from a surface ring crack. The results of a computer simulation indicated that the stress level generated at the target surface became the strength level of the material and that the shape coincided with that of the surface ring crack formed at the time of impact [25].

Durability Test [1]. A durability test was conducted under

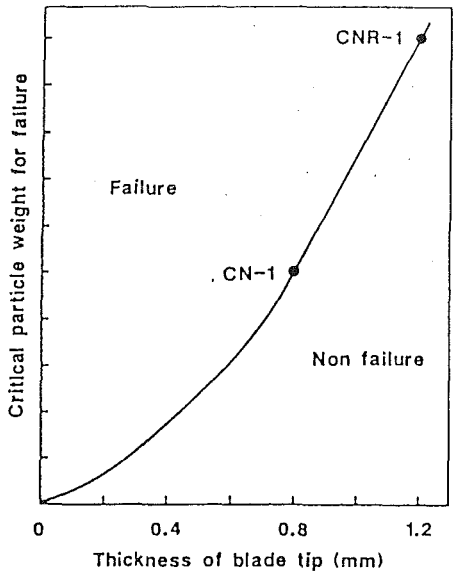

Fig. 17 Effect of blade tip thickness on dynamic strength

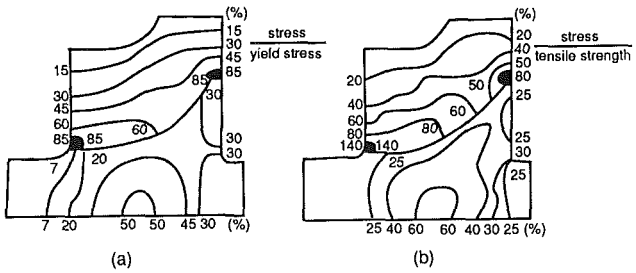

Fig. 18 Stress distributions for same rotor design: (a) metal (INCO 713C); (b) old ceramics (Si_3N_4); rotational speed: 145,000 rpm

real-world conditions using a spin impact tester. The relationship between the blade thickness at the turbine inlet and the particle load causing blade fracture is shown in Fig. 17. The dynamic strength of the turbine blade was determined by its thickness. Following these experiments, it was decided to make the thickness of the CNR-1 type turbocharger rotor 1.2 mm.

The following discussion describes some of the theories and techniques used in evaluating ceramic rotor reliability and in carrying out lifetime prediction and proof tests. Further details may be found in [1] and [27].

Reliability

According to Weibull's fracture theory, the failure probability of a ceramic component under a given stress can be found as

$$F = 1 - \exp[-(\sigma_r/\sigma_o)^m \cdot v_e] \tag{6}$$

where σ_r is the maximum stress in the ceramic component, σ_o is the characteristic strength, m is the Weibull modulus, and v_e is the effective volume. To lower the failure probability, it is necessary to reduce the stress that occurs in a ceramic component. This involves (1) reducing the level of maximum stress σ_r, (2) enhancing the material strength, i.e., increasing σ_o, and (3) reducing the variability in material strength, i.e., increasing the Weibull modulus, m. The work of developing a highly reliable turbocharger rotor was carried out on the basis of this concept.

The application of ceramics of structural components does not involve just a simple one-for-one replacement of metal materials. Figure 18 shows the results of a stress distribution

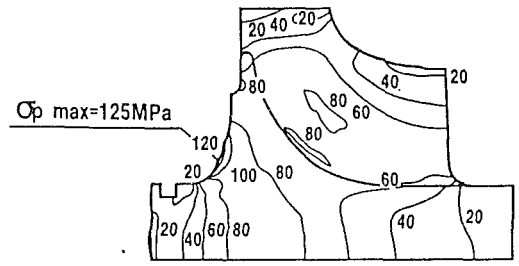

Fig. 19 Combined stress contours of rotor at steady state; rotational speed: 130,00 rpm, turbine inlet temperature: 900°C

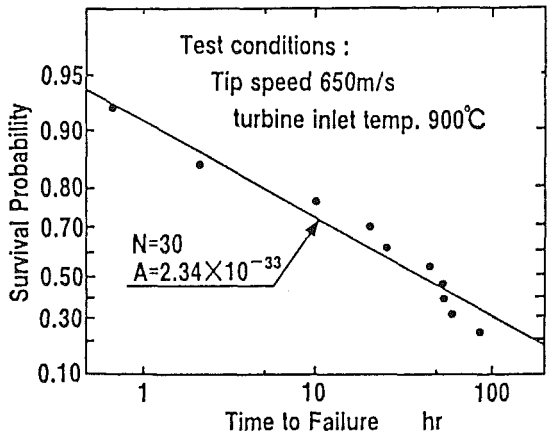

Fig. 20 Survival probability as a function of fatigue life

analysis when a ceramic material was used in place of a metal without changing the rotor design [26]. The results indicated that the shape should be changed in order to lower the maximum stress. This required a very detailed stress analysis. A three-dimensional finite element analysis technique was used in an effort to reduce stress in the ceramic rotor (Fig. 19) [28].

Lifetime Prediction

Slow crack growth under the temperature conditions of actual rotor usage is the dominant mechanism of static fatigue or delayed failure in ceramics. In general, it is though that a crack in a ceramic component grows to critical crack length under the occurence of stress, thereby giving rise to fracture. The lifetime of a component until an initial crack length a_i reaches the critical crack length a_c is given as

$$t_c = I[a_i^{(2-N)/2} - a_c^{(2-N)/2}] \tag{7}$$

where I is expressed as

$$I = 2/[A \cdot (N-2) \cdot Y^N \cdot \sigma_t^N] \tag{8}$$

and A and N are material constants determined by the conditions of component use, Y is shape factor, and σ_t is the stress generated under the conditions of use.

It is seen from these equations that component lifetime is determined by the initial crack length, critical crack length, applied stress, and the slow crack growth parameters A and N. However, as these values are also affected by the initial crack size and strength distribution under a condition of equal stress, it is necessary to apply statistical techniques to determine fracture probability in relation to applied stress and expected lifetime. The fracture probability of ceramic components exhibiting static fatigue can be calculated according to Weibull's theory. The initial strength distribution is correlated with the strength distribution of a fatigued material. The strength distribution of a fatigued component can be given by

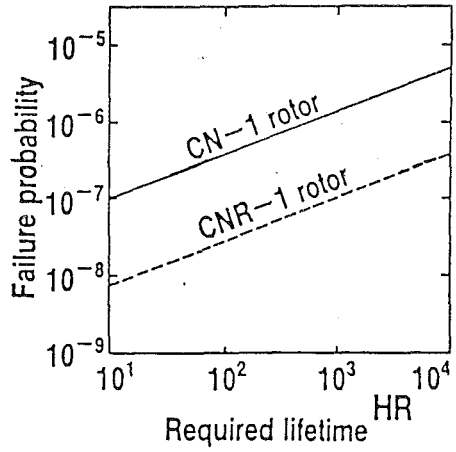

Fig. 21 Failure probability versus required lifetime

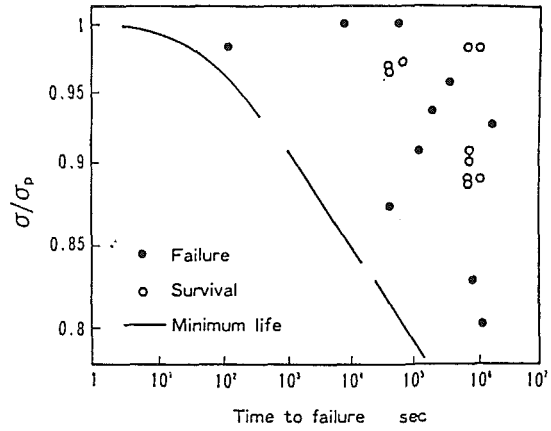

Fig. 22 Fatigue life after proof testing

$$\ln(-\ln P) = \{m/(N-2)\}\ln t_c + \{mN/(N-2)\}\ln \sigma + \{m/(N-2)\}\ln[\{(N-2)/2\}Y^2 \cdot A \cdot (K_{IC}/\sigma_o)^{N-2}] \quad (9)$$

where P is the survival probability and is equal to $1 - F$. The values of A and N can be found from this equation. This is accomplished by carrying out a test under a given stress level up to the point where failure occurs. The length of time to failure, t_c, is represented along the horizontal axis, while the survival probability is represented along the vertical axis. The value of N can be found from the slope of the characteristic curves and the value of A from their point of intersection.

Based on this approach, a test was conducted on an actual rotor at a turbine inlet temperature of 900°C and a constant tip speed of 650 m/s. The values of A and N found from experimental results are presented in Fig. 20. The same test was conducted on another rotor of the same shape but from a separated production lot having a different mean strength. Values of $N = 33$ and $A = 4.9 \times 10^{-34}$ were obtained. Since both exeriments yielded rather close values, it was verified that the values of A and N could be found from the results of rotational fatigue test conducted with actual rotors.

Using theses values of A and N, the relationship between lifetime and cumulative failure probability was calculated from Eq. (9). The results are shown in Fig. 21. The data indicate that the low-stress design of the CNR − 1 type rotor has lowered the failure probability by a factor of ten as compared with that of the CN − 1 type rotor provides high reliability with respect to component lifetime.

Proof Testing

Sintered ceramic bodies generally show a wide variety of initial defect size, and some cannot satisfy the failure probability requirement due to their initial crack length. At present, nondestructive evaluation to detect defects in complex shapes such as turbocharger rotors. An advance proof test is conducted by putting all sintered bodies under a momentary overloading condition exceeding the design stress. This approach is effective in excluding rotors whose initial defects are so large that they could not satisfy the lifetime and failure probability requirements.

The predicted minimum guaranteed lifetime is expressed as follows:

$$t_{\min} = 2/[(N-2) \cdot A - Y^2 \cdot K_{IC}^{N-2} \cdot \sigma^2 \cdot (\sigma/\sigma_p)^{N-2}] \quad (10)$$

where σ is the design stress and σ_p is proof stress. Figure 22 shows the results of rotational endurance experiments conducted on rotors that survived the proof test. The proof test results indicated that each rotor has a longer lifetime than the predicted minimum guaranteed lifetime and that the lifetime prediction method, based on the values of A and N obtained with actual rotors, was a valid approach. There were no cases where the proof test itself caused initial defects to exceed the allowable limits.

Conclusions

Techniques for applying for applying ceramics to turbocharger rotor were described with reference to investigations done by other researches. Since the mechanical properties of ceramics are sensitive to defects, it is essential to eliminate defects in the fabrication process as much as possible. The technology for joining ceramics and metals is a key factor is applying ceramics to structural components. It is known that residual machining damage degrades the mechanical strength of ceramics. This makes it necessary to determine the most suitable machining conditions for ceramics. Impact damage experiments provide useful information for determining design factors and assuring the durability of turbocharger materials. Reliability evaluation, lifetime prediction, and proof test evaluation are indispensable methodologies in the application of brittle ceramics to automotive turbocharger rotors.

References

1 Katayama, K., Watanabe, Y., Matoba, K., and Katoh, N., "Development of Nissan High Response Ceramic Turbocharger Rotor," Society of Automotive Engineers, Technical Paper No. 861128, 1986.

2 Matoba, K., Katayama, K., Kawamura, M., and Mizuno, T., "The Development of Second Generation Ceramic Turbocharge Rotor—Further Improvements in Reliability," Society of Automotive Engineers, Technical Paper No. 880702, 1987.

3 Matsuo, I., and Nishiguchi, F., "The Development of Second Generation Ceramic Turbocharger," Society of Automotive Engineers, Technical Paper No. 880703, 1987.

4 Ishida, T., Noguchi, M., Ura, S., Orita, M., Enomoto, M., and Hiasa, K., "The Development of New VG30 Twin Cam Ceramic Turbo Engine for CIMA," *Nissan-Gihou (Japan)*, Vol. 24, 1989, pp. 40-45 (s63-12).

5 Aida, M., Nakashima, M., Kawanishi, K., Ushigima, Y., Komatsu, H., and Goto, T., "Development of a Ball-Bearing Turbocharger," ibid., Vol. 25, 1989, pp. 48-54.

6 Ura, S., Nakamura, K., Fujita, H., Etoh, T., and Yamanaka, J., "The Development of the New RB26DETT Engine," ibid., Vol. 26, 1989, pp. 44-51.

7 Mutsuddy, B. C., and Shetty, D. K., "Injection Molding Ceramic Parts for High-Temperature Applications," *Technical Aspects of Critical Materials Used by the Steel Industry*, Vol. II-B, 1982, National Bureau of Standards.

8 Nikkei New Materials, No. 68, 1989, pp. 64-71.

9 Ito, M., Ishida, N., and Katoh, N., "Development of Brazing Technology for Ceramics Turbocharger Rotors," Society of Automotive Engineers, Technical Paper No. 880704, 1988.

10 Frank, F. C., et al., "On the Theory of Hertzian Fracture," *Proc. Roy. Soc. Ser. A*, Vol. 299, 1967, p.291.

11 Lawn, B. R., et al., "Indentation Fracture and Strength Degradation in Ceramics," *Fracture Mechanics of Ceramics*, Vol. 3, 1978, pp. 205-229.

12 Lawn, B. R., et al., "A Model for Crack Initiation in Elastic/Plastic Indentation Field," *J. Mat. Sci.*, Vol. 12, 1977, p.2195.

13 Kirchner, H. P., et al., "Fragmentation and Damage Penetration During

Abrasive Machining of Ceramics," *The Science of Ceramics Machining and Surface Finishing II*, N. B. S Special publication, Vol. 562, 1979, pp. 23–42.

14 Evans, A. G., et al., "Quasi-Static Solid Particle Damage in Brittle Solids I," *Acta Metallurgica*, Vol. 24, 1976, pp. 939–956.

15 Ratterman, E., *Ceramic Industry*, Feb. 1986.

16 Ohta, M., et al., "The Effect of Machining Condition to the Strength," *Proc. Autumn Meeting, Japan Engineering Society*.

17 Evans, A. G., "Strength Degradation by Projectile Impacts," *J. Am. Ceram. Soc.*, Vol. 56, 1973, pp. 405–409.

18 Dao, K. C., Shockey, D. A., Seaman, L., Curran, D. R., and Rowcliffe, D. J., "Particle Impact Damage in Silicon Nitride," Annual Reports, Part III, Office of Naval Research, Contract No. 0001476-057, May 1979.

19 Abou el-leil, M., Cammaratta, F., and Digenova, R. R., "Impact Fracture of Thermally Tempered Glass Helicopter Windshields," *J. Am. Ceram. Soc.*, Vol. 68, 1985, pp. c18–c21.

20 Liaw, B. M., Kobayashi, A. S., Emery, A. F., and Du, J. J., "An Impact Damage Model of Ceramic Coating, " in: *Fracture Mechanics of Ceramics*, Vol. 7, R. C. Bradt, A. G. Evans, D. P. H. Hasselman, and F. F. Lange, eds., Plenum Press, New York, 1986.

21 Hertz, H. R., *Hertz's Miscellaneous Papers*, Chaps. 5 and 6, McMillan, London, 1896.

22 Akimune, Y., Katano, Y., and Matoba, K., "Spherical Impact Damage and Strength Degradation in Silicon Nitride for Automobile Turbocharger Rotors," *J. Am. Ceram. Soc.*, Vol. 72, 1989, pp. 1422–1428.

23 Hallquist, J. O., "Theoretical Manual for DYNA3D," Lawrence Livermore Lab., W-7405-Eng-48, 1983.

24 Wiederhorn, S. M., and Lawn, B. R., "Strength Degradation of Glass Resulting From Impact With Spheres," *J. Am. Ceram. Soc.*, Vol. 60, 1977, pp. 451–458.

25 Akimune, Y., Izumi, T., Watanabe, S., and Tajima, Y., "Spherical Impact Damage in Sialon Ceramics for Turbine," *Proc. Annual Conference of Japan Ceramic Society High Temperature Division*, 1988, pp. 61–65.

26 Okazaki, Y., *Fine Ceramics Report*, Vol. 3, 1985, pp.16–23.

27 Sasaki, M., and Itoh, T., "Evaluation of Rotational Strength of Ceramic Gas Turbine Rotors and Development of Ceramic Turbocharger Rotors," *Journal of the Ceramic Society of Japan*, International Edition Vol. 97, R-1–12.

28 Itoh, T., "Reliability of Ceramic Turbocharger Rotor," *Ceramics*, Vol. 23, 1988, pp. 638–641, published by the Ceramic Society of Japan.